Publishing House
AKAPIT

COMPUTER METHODS IN MATERIALS SCIENCE
Informatyka w Technologii Materiałów

Vol. 17, 2017, No. 3

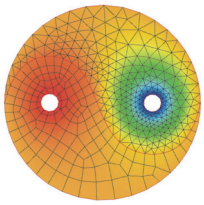

A COMPUTATIONAL FLUID DYNAMICS ANALYSIS OF TRANSPORT ENFORCED BY MARANGONI EFFECT DURING LASER WELDING

ALEKSANDER SIWEK

AGH University of Science and Technology,
Al. A. Mickiewicza 30, 30-059 Kraków, Poland
**Corresponding author: Aleksander.Siwek@agh.edu.pl*

Abstract

The presence of surface active elements such as sulfur in steel, changes the surface tension on the weld pool surface. The Marangoni effect induced by temperature dependent surface tension gradient, determines the direction of fluid flow in the entire volume of the weld pool. The difference of initial sulfur concentration of the welded parts is an additional factor which complicates the model. During welding an additional body force source term has been added to the momentum equations at the liquid steel surface, depending on sulfur concentration gradient. Mutual mixing of welded steels in the weld pool leads to periodic changes of driving force direction. The model permits the calculation of sulfur concentration in the weld pool and weld size depending on the initial composition, laser power and welding velocity.

Key words: CFD, dissimilar welding, surface active element

1. INTRODUCTION

Joining metals and alloys with different properties gives greater flexibility in design and production as compared to manufacturing with one type of material only. As the result, expensive materials can be applied only at places where their use is indispensable. Hybrid structures with different classes of materials increase product features and performance (Martinsen et al., 2015). However, joining different combinations of metals become a challenge, due to the differences in physical and chemical properties. In the fabrication and manufacturing industry many joining methods of dissimilar materials are used, e.g.:

- inertia friction welding where the coalescence of materials is obtained through pressure and relative motion of the two workpieces (D'Alvise et al., 2002),
- friction stir welding where heat is generated by friction between the rotating non-consumable tool and materials (Meshram et al., 2007; Dörfler, 2008; DebRoy & Bhadeshia, 2010; Salimi et al., 2014),
- gas tungsten arc welding of dissimilar metals under argon shielding gas is an effective and inexpensive technique (Tinkler et al., 1984; Mishra et al., 2008; Bahrami et al., 2015),
- spot welding where heat balance must be achieved in order to compensate difference in metals properties (Darwish, 2004),
- laser spot joining where reaction between two alloys results in intermetallic compounds (Pardal et al., 2014),
- laser welding which features such advantages as good weldability and high quality of joints with narrow heat affected zone, allows for solving many problems present in appearing in other

 ISSN 1641-8581

joining methods (Sun & Ion, 1995; Yao et al., 2009; Lienert et al., 2014; Hu et al., 2012).

The spatial gradient of surface tension during laser welding affects the heat and mass transfer in the weld pool (Zhao et al., 2010). Difference in the content of surface active elements in the welded plates significantly changes the shape of the weld pool. The weld joint becomes asymmetric to the surface of the materials contact. Asymmetry depends also on the welding speed and distance between laser beam and contact surface (Tomashchuk et al., 2013). This process can be analyzed by the numerical modeling of the heat and mass transfer during welding of steel plates with different sulfur content. Laser power and laser beam mod also affect this process (Han & Liou, 2014).

This paper concerns modelling of laser welding processes for steels with different physical properties. The model consists of a coupled set of incompressible fluid flow equation, heat transfer equation and advection-diffusion equation for different steel grades. The formulation takes into account the dependence of material properties on temperature and chemical composition. Discontinuity of density and viscosity, together with the chemical composition of fluid in the weld pool influences the fluid velocity and temperature distribution in the weld pool and in consequence determines the shape and properties of a joint. Analysis includes the dependence of the weld pool size and shape on the composition of joined steels and welding parameters.

2. MATHEMATICAL MODEL

The following assumptions are made in the model:

- welded steels behave in liquid state as a Newtonian incompressible fluid,
- alloys exhibit unlimited solubility in the solid and liquid state,
- the weld pool surface remains flat
- the flow in the weld pool is turbulent for high laser power, turbulence is simulated using the standard k-ε model,
- motion of the liquid in the weld pool is induced by the gradient of surface tension.

The model described in this article consists of two plates with different compositions. The welding model is based on several differential equations of mass, momentum, energy and species conservation. Each equation requires initial and boundary conditions. Boundary conditions on the surface of the weld pool are given by (Mishra et al., 2008; Hu et al., 2012):

$$\begin{aligned} \mu\frac{\partial u}{\partial z} &= f_l\left(\frac{\partial\gamma}{\partial T}\frac{\partial T}{\partial x}+\frac{\partial\gamma}{\partial c_i}\frac{\partial c_i}{\partial x}\right)\\ \mu\frac{\partial v}{\partial z} &= f_l\left(\frac{\partial\gamma}{\partial T}\frac{\partial T}{\partial y}+\frac{\partial\gamma}{\partial c_i}\frac{\partial c_i}{\partial y}\right)\\ w &= 0 \end{aligned} \tag{1}$$

where u, v, w are velocity components in x, y and z directions, μ is the viscosity, f_l is the volume of fluid fraction, $\partial\gamma/\partial T$ and $\partial\gamma/\partial c_i$ are temperature and concentration coefficients of surface tension. Since the initial concentration of the surface active element in each plate is different, the non-zero gradient of concentration exists on the weld pool surface (Bahrami et al., 2015). Surface tension given by the equations (1) forces liquid motion in x and y directions. The model assumes a flat surface of the weld pool. Therefore w component of the velocity remains null on the weld pool surface ($z = 0$).

Surface tension of the steel depends on both temperature and surface active element as follows (Sahoo et al., 1988):

$$\gamma = \gamma_m^\circ - A(T-T_m) - \mathrm{R}\,T\,\Gamma_s \ln\left[1+k_1\,c_i e^{-(\Delta H^\circ/\mathrm{R}\,T)}\right] \tag{2}$$

where γ_m° is the surface tension of pure metal at the melting point, A is the negative of the $\partial\gamma/\partial T$ for pure metal, T_m is the melting point of the material, Γ_s is surface excess at saturation, k_1 is a constant related to the entropy, c_i is the concentration of the surface active element, ΔH° is the standard heat of adsorption.

The temperature coefficient of surface tension $\partial\gamma/\partial T$ can be calculated by differentiating equation (2) with respect to temperature (Sahoo et al., 1988):

$$\begin{aligned} \frac{\partial\gamma}{\partial T} &= -A - \mathrm{R}\,\Gamma_s \ln\left[1+K\,c_i\right] - \frac{K\,c_i}{(1+K\,c_i)}\frac{\Gamma_s\,\Delta H^\circ}{T}\\ K &= k_1\,e^{-(\Delta H^\circ/\mathrm{R}\,T)} \end{aligned} \tag{3}$$

Temperature coefficient of surface tension is a function of temperature and concentration of the surface active element. For pure metals $\partial\gamma/\partial T$ is negative but the growth of surface active elements concentration (eg. sulphur, oxygen), changes the sign to positive (Sahoo et al., 1988). This in turn results in change of fluid flow direction and shape of the weld pool.

In this paper modeling investigation of laser welding of stainless steel plates with different sulfur concentrations is presented. Materials data necessary for calculation of temperature coefficient of surface tension are listed in table 1. Based on these data and equation (3), the relationship between $\partial\gamma/\partial T$ and temperature for three sulfur concentrations is shown in figure 1. As can be seen in figure 1, the temperature coefficient $\partial\gamma/\partial T$ decreases together with the temperature growth, for all sulfur concentrations. However, it is important to note that together with the temperature growth the coefficient $\partial\gamma/\partial T$ changes its sign which results in the reverse direction of the fluid flow. When the sulfur concentration increases, the temperature at which the coefficient $\partial\gamma/\partial T$ changes its sign increases as well. The value and the sign of the temperature coefficient determine the shape of the weld pool. Negative sign of $\partial\gamma/\partial T$ coefficient causes fluid flow from high (laser beam center) to the low temperature surface (boundary of the weld pool). Then heat supplied to the melt is transported mainly to the weld pool boundary. This results in wide and shallow weld pool. Positive sign of $\partial\gamma/\partial T$ coefficient forces the liquid flow from the boundary (low temperature) to the center of the weld pool (high temperature). There, the welding heat is directed from the surface to the bottom of the weld pool. Such type of liquid metal flow creates a deep weld of smaller width.

Table 1. *Physical properties of the steel used in the calculations (Touloukian, 1970; Sahoo et al., 1988).*

Physical property	Value	
Liquidus temperature, T_l	1686	K
Solidus temperature, T_s	1767	K
Density, ρ	7750	kg/m^3
Specific heat of solid, C_{ps}	680	J/kg K
Specific heat of liquid, C_{pl}	820	J/kg K
Thermal conductivity of solid, k_s	25	W/m K
Thermal conductivity of liquid, k_l	20	W/m K
Viscosity of fluid, μ_l	$5.5\cdot10^{-3}$	kg/m s
Temperature coefficient of surface tension, A	$-0.43\cdot10^{-3}$	N/m K
Surface excess at saturation, Γ_s	$0.13\cdot10^{-6}$	mol/m^2
Entropy factor, k_1	$3.18\cdot10^{-3}$	-
Enthalpy of adsorption, $\Delta H°$	$-166.2\cdot10^{3}$	J/mol
Absorption coefficient, η	0.13	-
Radiation coefficient, ε	0.6	-

The model of the welding process described in this article assumes different concentrations of active elements in plates. Concentration coefficient of surface tension is obtained by differentiating equation (2) with respect to concentration:

$$\frac{\partial\gamma}{\partial c_i} = -\frac{\mathrm{R}\,T\,\Gamma_s\,K}{(1+K\,c_i)} \tag{4}$$

A non-zero gradient of sulfur concentration at the steels interface implies non-zero second terms of right hand side of equations (1). For the materials data listed in table 1 and equation (4), figure 2 shows dependence of coefficient $\partial\gamma/\partial c_i$ on the sulfur concentration for three temperatures. As can be seen in figure 2, the absolute value of $\partial\gamma/\partial c_i$ decreases together with the increase of temperature and sulfur concentration. A negative value of this coefficient induces a tangential shear stress that tends to uniform sulfur concentration on the weld pool surface.

In this study a computational fluid dynamics (CFD) code ANSYS Fluent was used to solve conservation equations and advection-diffusion equation of sulfur concentration (Fluent, 2016). The Fluent is a finite volume software based on the weighted residuals (Patankar, 1980). The model of laser welding processes is represented as a schematic workflow on flowchart diagram. The model is composed of the three blocks called systems:

- Mesh: software that includes tools for meshing of the model
- Fluent preprocessor and solver, providing ability to set boundary conditions, define fluid properties and execute the solution,
- Results: system of visualization and quantitative analysis of the results of CFD simulations.

A tetrahedral unstructured mesh was applied, refined in the weld area to ensure an adequate accuracy. The source terms in heat and momentum equations defined in C by User Defined Functions (UDF) was then hooked to the CFD model (Fluent, 2016). During welding heat source moves with constant velocity in direction parallel to the steels interface.

The energy balance at the model top surface is calculated as follows:

$$k\frac{\partial T}{\partial \mathbf{n}} = \eta\,\Phi_{las} - \varepsilon\,\sigma(T^4 - T_o^4) - h(T - T_o) - q_{evap} \tag{5}$$

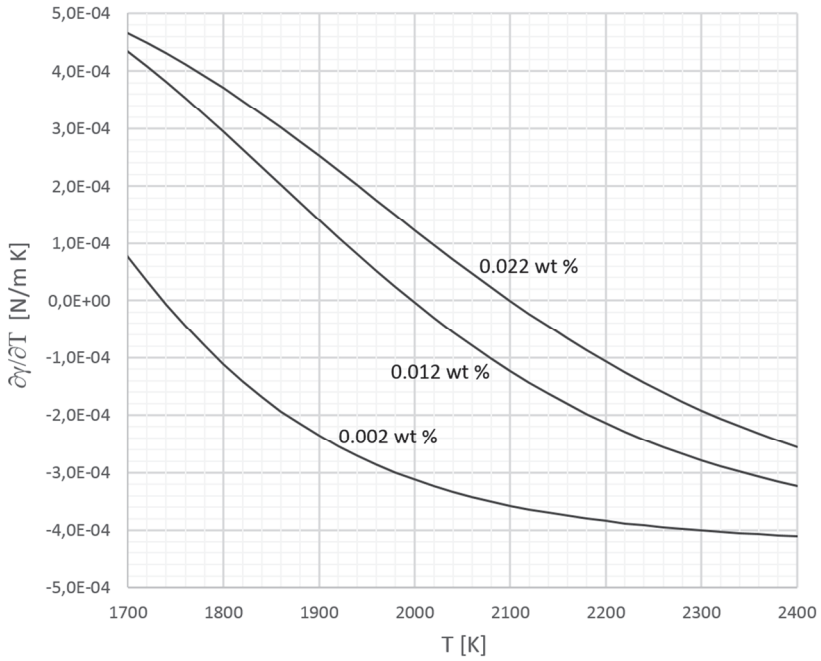

Fig. 1. *Temperature coefficient of surface tension $\partial\gamma/\partial T$ as a function of temperature T and sulfur concentration (wt.%).*

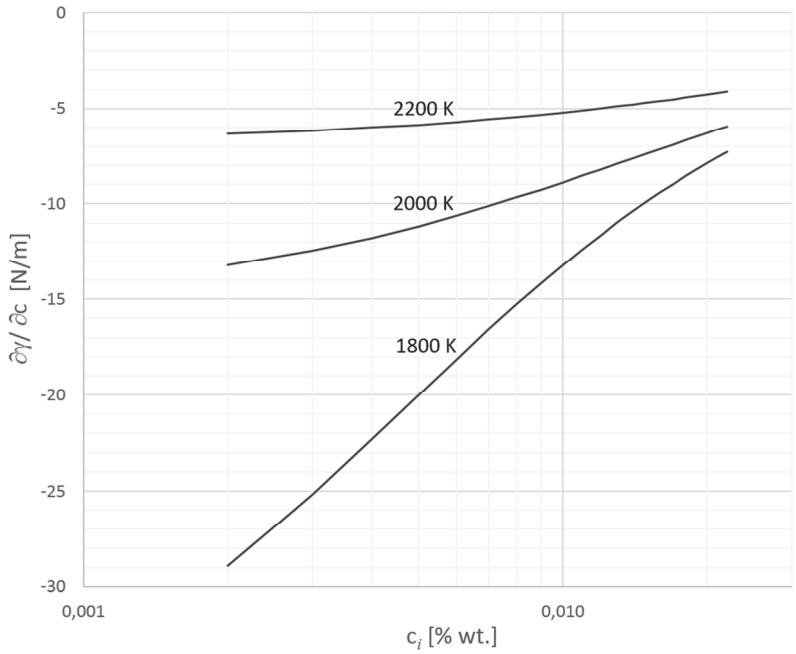

Fig. 2. *Concentration coefficient of surface tension $\partial\gamma/\partial c$ as a function of sulfur concentration c_i for temperatures 1800, 2000 and 2200 K.*

where **n** is a unit vector normal to the surface, Φ_{las} is the Gaussian intensity distribution for the laser beam mode TEM_{00} (Han & Liou, 2014), η is the absorption coefficient, ε is the radiation coefficient, σ is the Stefan-Boltzmann constant, T_o is the ambient temperature, h is the convective coefficient, q_{evap} is the evaporation heat loss calculated by Zacharia et al. (1991). The second, third and fourth term in equation (5) are the energy loss due to the radiation, convection and evaporation. The energy balance at the other model surfaces comprise only convection term.

An advection-diffusion equations of surface active element composition are solved using User Defined Scalars (UDS). The standard SIMPLE algorithm (Semi-Implicit Method for Pressure-Linked Equation) is employed for updating pressure and correcting velocity components to ensure mass conservation at each time step (Ferziger & Perić, 2001). Table 1. summarizes materials data used for numerical simulation. In the mushy zone temperature range between solidus and liquidus temperature, linear approximation of materials data are employed.

3. PROBLEM FORMULATION

The model consists of two plates with different sulfur concentrations (figure 3). The plates are of the same size $2\times4\times1\cdot10^{-3}$ m and are tightly adherent to each other. The laser beam moves at a constant velocity in a direction parallel to the contact plane between plates. The welded parts were initially at ambient temperature. Welding conditions of tests are listed in Table 2. Due to convergence of the solution for the assumed process conditions, constant time step $\Delta t=10^{-6}$ s is adopted, whereas the size of the tetrahedral elements is reduced from the size $\sim10^{-4}$ m in the outer region of the welded plates, to the size $\sim3\cdot10^{-5}$ m in the vicinity of the laser beam. Further reducing the size of the mesh makes no significant change in the shape and size of the weld pool.

Table 2. *Conditions set in the welding tests.*

Test number	Left plate, sulfur [wt.%]	Right plate, sulfur [wt.%]	Laser power, P [W]	Welding speed v [mm/s]
1	0.002	0.0220	1000	5.0
2	0.002	0.0220	1500	5.0
3	0.002	0.0220	2000	5.0

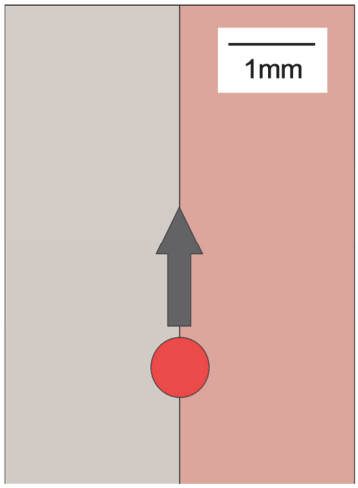

Fig. 3. Schematic view of the laser welding model.

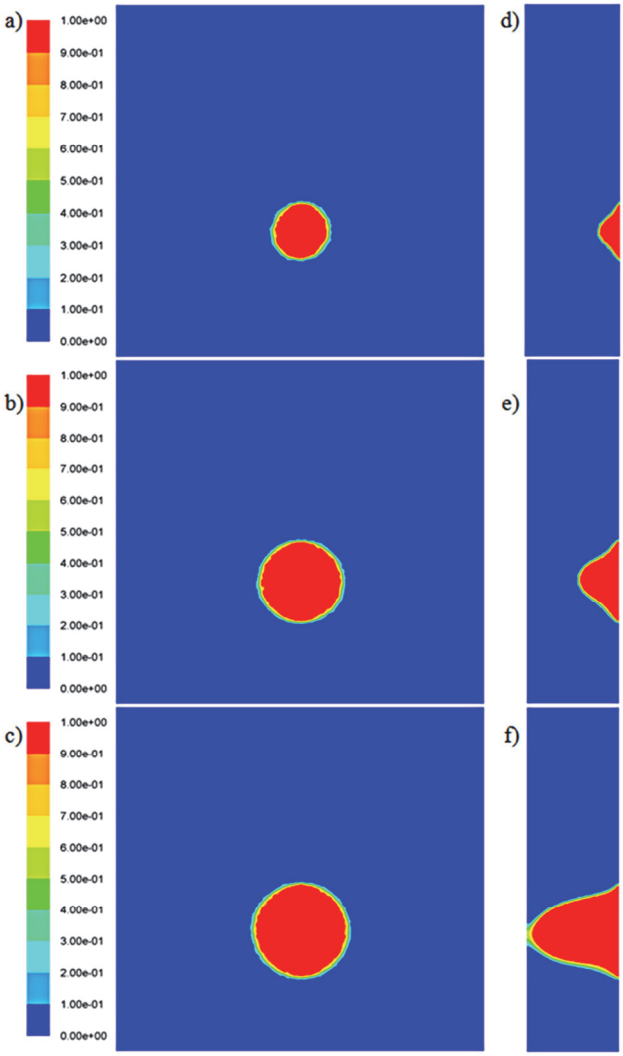

Fig. 4. Liquid fraction for a welding time t=0.194s. The laser beam power 1000W (a,d), 1500W (b,e) and 2000W (c,f). The upper surface view (a-c) and longitudinal section view (d-f)

4. NUMERICAL RESULTS

A number of tests have been carried out to investigate the effect of sulfur concentration on the welding process. The selected welding parameters are listed in Table 2. The sulfur concentration of the left plate is 0.002 wt.% and for the right plate 0.022 wt.%. For such range of sulfur concentration, temperature coefficient of the surface tension changes the sign in a wide range of temperature (figure 1). Welding speed and laser beam power determine the amount of energy supplied per unit length of the weld at each time step. The simulation is stopped when the laser reaches the opposite side of the plates or earlier, when the liquid appears at the bottom surface. For the laser beam power of 2000W the weld pool full penetration was achieved at the welding time $t = 0.194$s. Figures 4 and 5 contain simulation results for the tests 1-3 (table 2). The temperature and concentration distribution on the weld pool surface results in surface tension gradient. Marangoni force acting on central part of the weld pool surface results in radially inward fluid flow. In the area near the edge of the weld pool, Marangoni force and fluid flow are outward from the laser beam axis. This system of forces on the weld surface causes fluid convection inside the weld pool, forming bendings of the mushy zone (figs. 4d, 4e, 4f). In the initial phase of the welding, the weld pool appears in the centre of the laser beam. The width of this zone grows and reaches a maximum value. The maximal width of the molten pool increases with the increase of the laser beam power. The width is 0.71mm for laser power 1000W, 0.94mm for 1500W and 1.13mm for 2000W. For the conditions adopted in tests 1-3, there is no evidence of the weld pool shift or rotation relative to the original joint interface described in Rollin and Bentley (1984), Tinkler et al. (1984), Lienert et al. (2014), Wei et al. (2015).

During each time step iteration advection-diffusion equation of sulfur concentration is solved. Figure 5 shows the distribution of sulfur after the welding time $t = 0.194$s. Isoconcentration lines create an undulating pattern upon the weld surface. At the animation available on the web site Siwek (2017) we can see the weld pool formation and variation of the sulfur distribution. In front of the weld pool in the plate containing 0.022wt.% of sulfur, a flat mixing front is formed. In the middle there is a liquid metal stream formed and directed towards

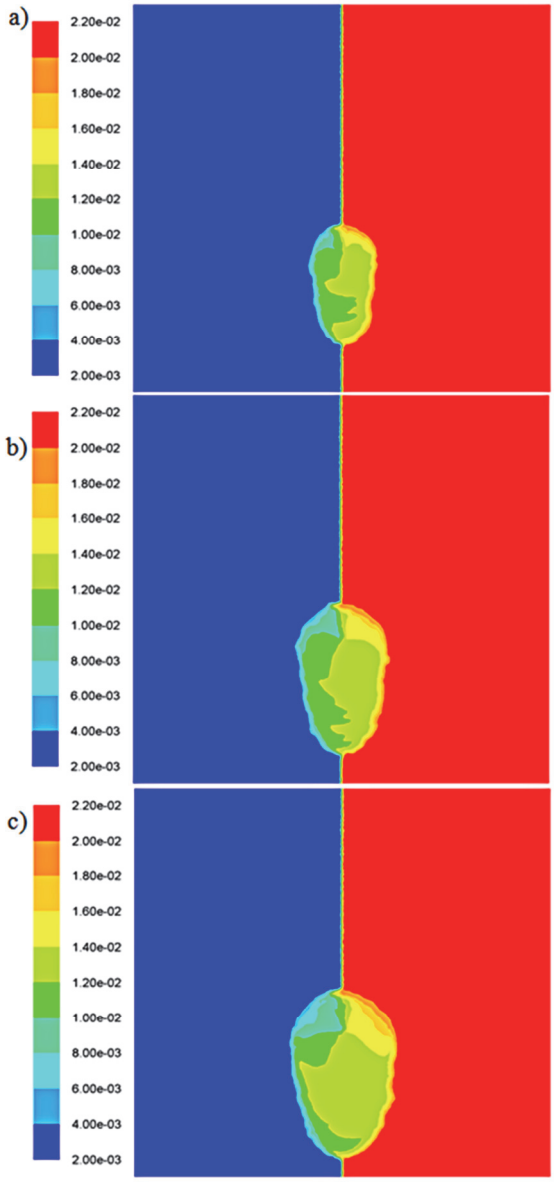

Fig. 5. *Distribution of the sulfur concentration (wt.%) for a welding time t=0.194s on the upper surface of the plate. The laser beam power 1000W (a), 1500W (b) and 2000W (c).*

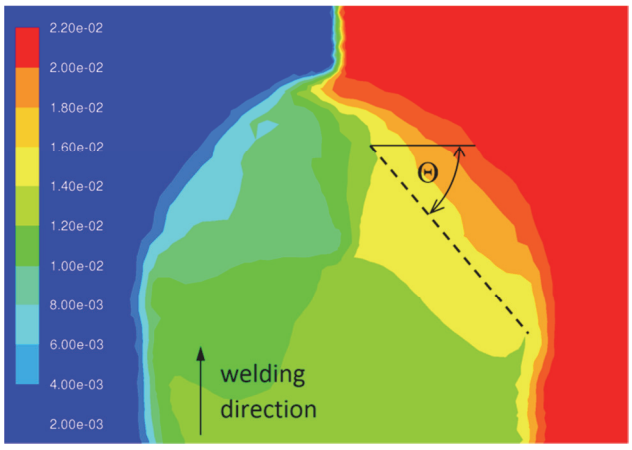

Fig. 6. *Mixing front (dotted line) formed in the plate irradiated by laser beam of power 2000W. The slope of the mixing front (Θ) measured in relation to welding direction.*

the laser beam axis (figure 6). The slope of the mixing front increases together with the laser power increase (figure 7). Such surface flow may promote the rotated elliptical shape weld pool. For the welding conditions, such effect is not observed. The driving force of fluid flow on the weld pool is the surface tension (equations 1). Temperature and sulfur concentration on the surface both determine the value and direction of this force. Forced convection of liquid metal on the weld pool surface causes inflection of the sulfur concentration curves (figure 8a). Central inflection is formed by the inward convection on the surface. External inflections are the effect of outward convection at the edge of the weld pool. In the direction of the laser movement in front of the beam axis, the fluid becomes increasingly poorer in sulfur with the increase of the laser power (figure 8b). While behind axis sulfur distribution in fluid is opposite.

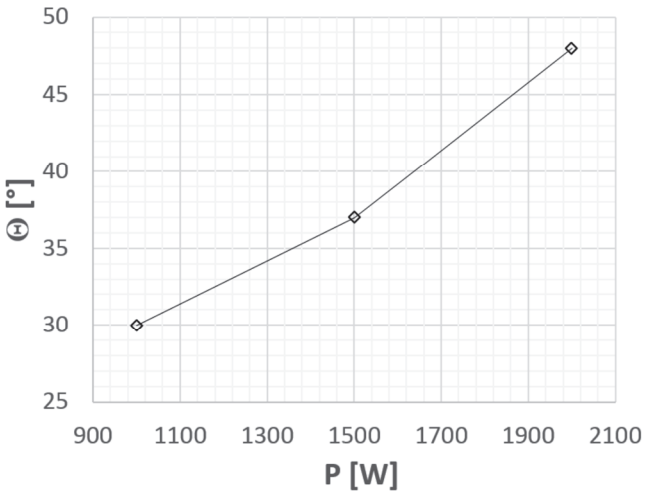

Fig. 7. *Dependence of the mixing front slope (Θ) on the laser beam power (P).*

For the welding conditions investigated in this research on the surface of the weld pool, there is a non-zero gradient of sulfur concentration. The largest gradient is at the edge of the weld pool. However, sulfur gradient is greater in the plate with higher sulfur content. While concentration coefficient of surface tension $\partial\gamma/\partial c$ takes only negative, the absolute value of $\partial\gamma/\partial c_i$ decreases with the increasing temperature and sulfur concentration (figure 2). Therefore, coefficient $\partial\gamma/\partial c$ reaches absolute largest value at the weld pool edge in the plate with lower sulfur content (figure 9a). The influence of sulfur distribution on the driving force of fluid flow gives second terms in equations 1. The product of the sulfur gradient and coefficient $\partial\gamma/\partial c$ gives driving force, largest at the weld pool edge.

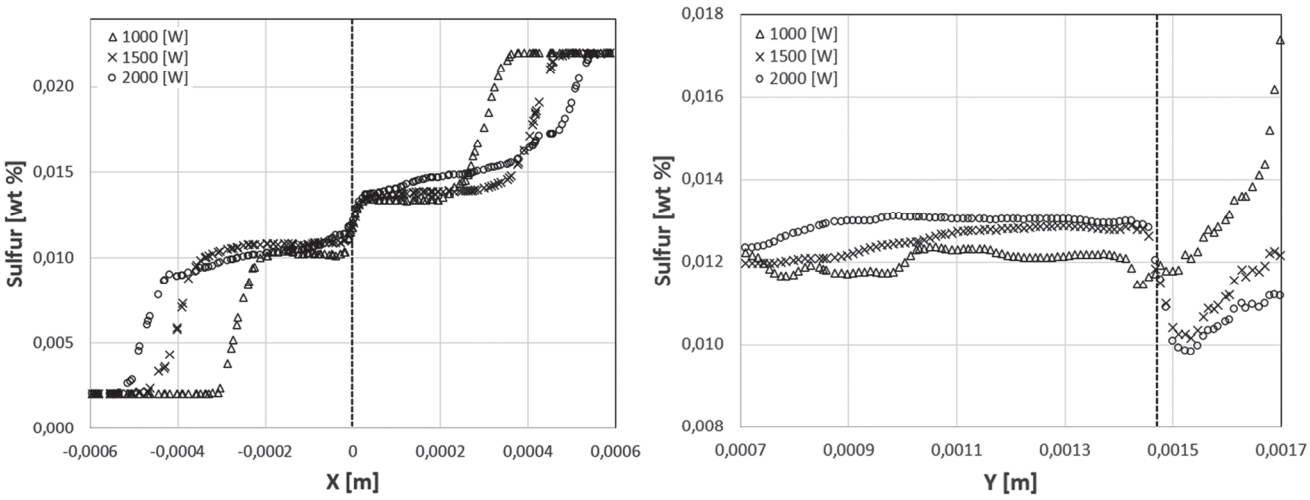

Fig. 8. Distribution of the sulfur concentration on the weld pool surface in direction perpendicular (a) and parallel (b) to the welding direction (t=0.194s). The laser beam axis position indicated as dashed line.

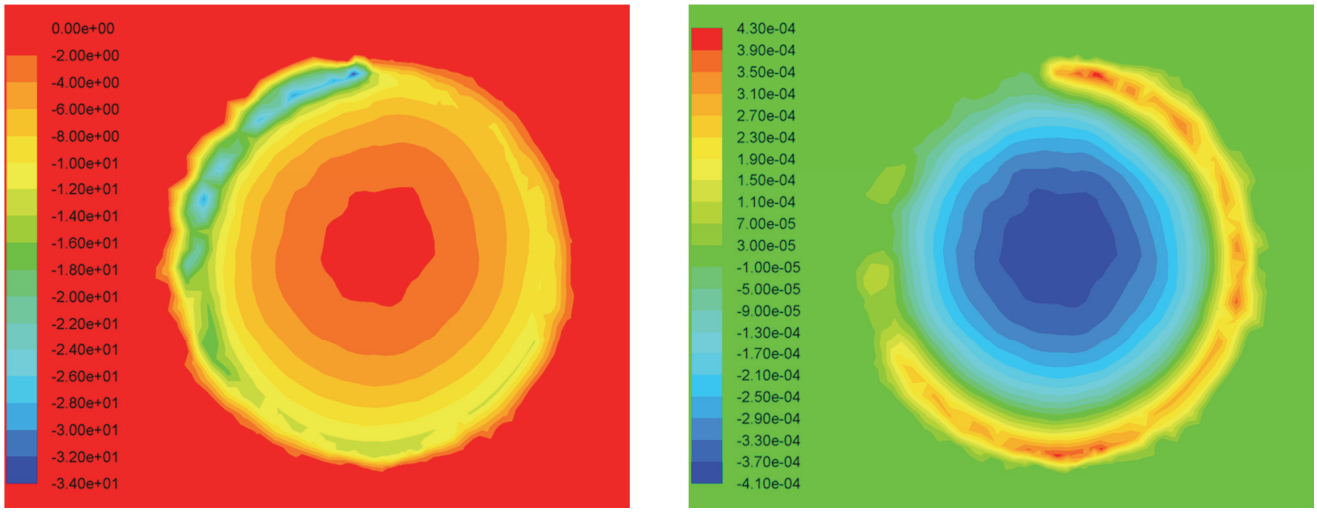

Fig. 9. Distribution of the surface tension coefficient $\partial\gamma/\partial c$ (a) and $\partial\gamma/\partial T$ (b) on the weld pool surface (t=0.194s).

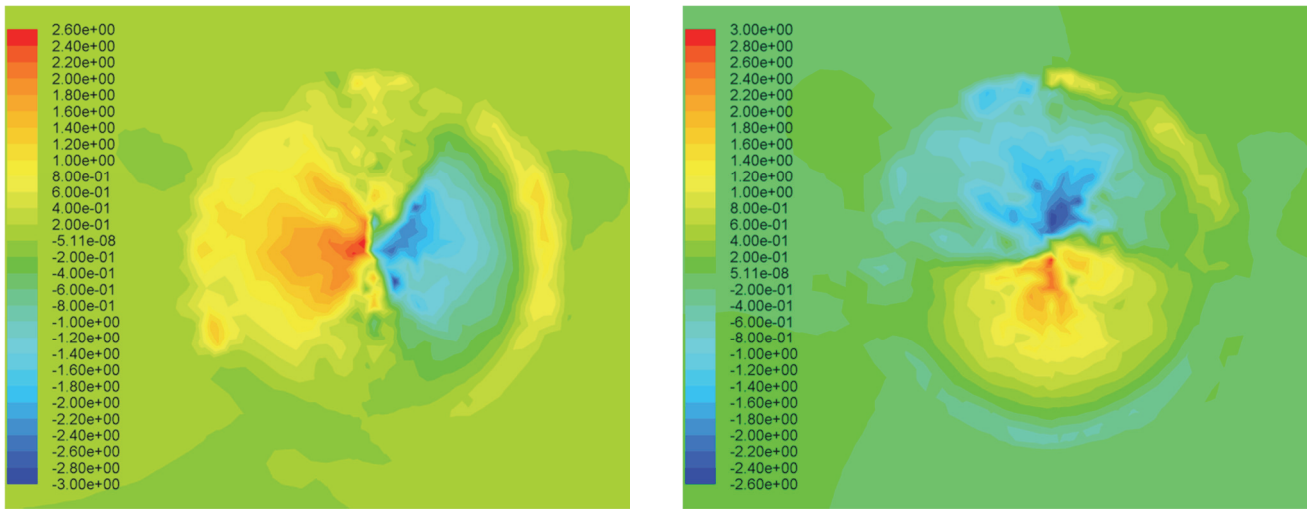

Fig. 10. Distribution of the velocity component u (a) and v (b) on the weld pool surface (t=0.194s).

The temperature gradient upon the weld pool surface is the highest in its inner part. In this area, the magnitude and direction of the driving force varies with temperature and sulfur content. Temperature coefficient of surface tension $\partial\gamma/\partial T$ is negative for lower sulfur content and higher temperature, while positive for higher sulfur content and lower temperature (figure 1). Therefore coefficient $\partial\gamma/\partial T$ reaches minimum in the inner part of the pool, where temperature is high and by convection sulfur content is low (figure 9b). Coefficient $\partial\gamma/\partial T$ reaches maximum at the weld pool edge where the sulfur content is highest. Strong convective mixing of sulfur in the weld pool causes dynamic sign changes of $\partial\gamma/\partial T$ coefficient. The product of temperature gradient and $\partial\gamma/\partial T$ coefficient gives driving force, largest in the inner part of the weld pool.

Combined action of the above described forces decide on velocity field of fluid on the pool surface. Figure 10 shows the velocity components of the liquid on the surface. In the inner part of the weld pool surface the liquid flow is directed towards the laser beam axis. Close to the laser beam axis it changes its directions and goes downwards to the weld pool. Such velocity field gives deeper melting. At the weld pool edge, a narrow zone with an outward flow is observed. Only in a part of this zone (limited 9 and 12 hour clock) the fluid flows radially inwards. In this area coefficient $\partial\gamma/\partial T$ is close to zero (figure 9b) and coefficient $\partial\gamma/\partial c$ is lowest negative (figure 9a).

5. CONCLUSIONS

As far as the welding parameters are concerned no weld pool shift or rotation relative to the original joint interface was observed during the laser welding of steel plates with different sulfur concentration. Mixing of the sulfur from the plates, changes the gradient vector field of the sulfur. The Marangoni stress caused by difference of surface tension gives the asymetry of the velocity field. The difference of initial sulfur concentration significantly influences the fluid velocity field.

The numerical modelling of fluid flow, heat transfer and advection-diffusion allows tracking the sulfur concentration during welding. Isoconcentration lines create characteristic pattern on the weld pool during welding. This proves the existence of a periodic changes in surface tension. This is the main driving force of fluid flow in a weld pool. Therefore, the width and depth of the weld may also be subject to periodic changes during welding.

ACKNOWLEDGEMENTS

This research was supported by financial assistance of MNiSzW in the framework agreement 11.11.110.300 and by PL-Grid Infrastructure.

REFERENCES

D'Alvise L., Massoni, E., Walløe, S.J., 2002, Finite element modelling of the inertia friction welding process between dissimilar materials, *Journal of Materials Processing Technology* 125–126, 387-391.

Darwish, S.M., 2004, Analysis of weld-bonded dissimilar materials, *International Journal of Adhesion & Adhesives*, 24, 347-354.

DebRoy, T., Bhadeshia, H.K.D.H., 2010,Friction stir welding of dissimilar alloys – a perspective, *Science and Technology of Welding and Joining*, 15(4), 266-270.

Dörfler, S.M., 2008, Advanced modeling of friction stir welding – improved material model for aluminum alloys and modeling of different materials with different properties by using the level set method, *Proceedings of the COMSOL Conference*, Hannover.

Ferziger, J.H., Perić, M., 2002, *Computational Methods for Fluid Dynamics*, Springer-Verlag, Berlin.

Fluent. Inc. Fluent 17.2, *User's guide*, 2016.

Hann, L., Liou, F.W., 2014, Numerical investigation of the influence of laser beam mode on melt pool, *International Journal of Heat and Mass Transfer*, 47, 4385-4402.

Hu, Z., He, X, Yu, G., Ge, Y., Zheng, C., Ning, W., 2012, Heat and mass transfer in laser dissimilar welding of stainless steel and nickel, *Applied Surface Science*, 258, 5914-5922.

Lienert, T.J., Burgardt, P., Harada, K.L., Forsyth, R.T., DebRoy T., 2014, Weld bead center line shift during laser welding of austenitic stainless steels with different sulfur content, *Scripta Materialia*, 71, 37-40.

Martinsen K., Hu S.J., Carlson B.E., 2015, Joining of dissimilar materials, *CIRP Annals - Manufacturing Technology*, 64, 679-699.

Meshram, S.D., Mohandas, T., Reddy, G.M., 2007,Friction welding of dissimilar pure metals, *Journal of Materials Processing Technology*, 184, 330-337.

Mishra, S., Lienert, T.J., Johnson, M.Q., DebRoy, T., 2008, An experimental and theoretical study of gas tungsten arc welding of stainless steel plates with different sulfur concentrations, 56, 2133-2146.

Pardal, G., Meco, S., Ganguly, S., Williams, S., Prangnell, P., 2014, Dissimilar metal laser spot joining of steel to aluminium in conduction mode, *Internationa Journal of Advanced Manufacturing Technology*, 73, 365-373.

Patankar, S.V., 1980, *Numerical Heat Transfer*, McGraw-Hill, New York.

Rollin, A.F., Bentley, M.J., 1984, Weldability of nuclear components - the effects of minor cast variations, *Proceedings of the International Conference on the Effects of Residual, Trace and Microalloying Elements*

on Weldability and Weld Properties, ed. P.H.M. Hart, Cambridge, 273-280.

Sahoo, R., DebRoy, T., McNallan, M.J., 1988, Surface tension of binary metal surface active solute systems under conditions relevant to welding metallurgy, *Metallurgical Transactions B*, 19B, 483-491.

Salimi, S., Bahemmat, P., Haghpanahi, M., 2014,A 3D transient analytical solution to the temperature field during dissimilar welding processes, *International Journal of Mechanical Sciences*, 79, 66-74.

Siwek, A., 2017, Laser welding simulation, http://home.agh.edu.pl/asiwek/welding, accessed: 2.06.2017.

Sun, Z., Ion, J.C., 1995, Review, Laser welding of dissimilar metal combinations, *Journal of Materials Science*, 30, 4205-4214.

Tinkler, M.J., Grant, I., Mizuno, G., Gluck, C., 1984, Welding 304L stainless steel tubing having variable penetration characteristics, *Proceedings of the International Conference on the Effects of Residual, Trace and Microalloying Elements on Weldability and Weld Properties*, ed. P.H.M. Hart, Cambridge, 247-258.

Tomashchuk, I., Sallamand, P., Jouvard, J.M., 2013, The modeling of dissimilar welding of immiscible materials by using a phase field method, *Applied Mathematics and Computation*, 219, 7103-7114.

Touloukian, Y.S., 1970, *Thermophysical properties of matter*, IFI/Plenum, New York.

Wei, H.L., Pal, S., Manvatkar, V., Lienert, T.J., DebRoy, T., 2015, Asymmetry in steel welds with dissimilar amounts of sulfur, *Scripta Materialia*, 108, 88-91.

Yao, C., Xu, B., Zhang, X., Huang, J., Fu, J., Wu, Y., 2009,Interface microstructure and mechanical properties of laser welding copper–steel dissimilar joint, *Optics and Lasers in Engineering*, 47, 807-814.

Zacharia, T., David, S.A., Vitek, J.M., 1991, Effect of evaporation and temperature-dependent material properties on weld pool development, *Metallurgical Transactions B*, 22B, 233-241.

Zhao, C.X., Kwakernaak, C., Pan, Y., Richardson, I.M., Saldi, Z., Kenjeres, S., Kleijn, C.R., 2010, The effect of oxygen on transitional Marangoni flow in laser spot welding, *Acta Materialia*, 58, 6345-6357.

WYKORZYSTANIE OBLICZENIOWEJ MECHANIKI PŁYNÓW DO ANALIZY PRZEPŁYWU WYMUSZONEGO EFEKTEM MARANGONIEGO W CZASIE SPAWANIA LASEROWEGO

Streszczenie

Wpływ zawartości siarki na proces spawania opisany został w wielu pracach. Siarka jako jeden z pierwiastków powierzchniowo aktywnych wpływa na napięcie powierzchniowe stali. W większości publikacji dotyczących modelowania procesu spawania, zawartość siarki była taka sama w obydwu spawanych elementach. Artykuł dotyczy przypadku, gdy spawane stalowe elementy różnią się zawartością siarki. Mieszanie się spawanych stali w jeziorku spawalniczym prowadzi do okresowych zmian kierunku działania siły wymuszającej przepływ. Model pozwala na obliczenie rozkładu zawartości siarki w spoinie oraz wielkości spoiny w zależności od danych termofizycznych stali, początkowej zawartości siarki, mocy wiązki lasera i prędkości spawania.

Received: March 7, 2017
Received in a revised form: June 2, 2017
Accepted: July 31, 2017